Numerical analysis of the pressure gradient driven MHD flow in magnetically confined plasma using OpenFOAM

Author: Robert Benassai Dalmau
Facultat de Física, Universitat de Barcelona, Diagonal 645, 08028 Barcelona, Spain.

Advisors: Dr. Shimpei Futatani & Dr. Assumpta Parreño

Abstract: Numerical simulations of magnetohydrodinamical (MHD) flow of a magnetically confined plasma in a cylindrical geometry have been performed. The externally imposed magnetic field is formed in a helical configuration which is composed of axial and poloidal magnetic fields. The parametric scan of the magnetic fields shows that the intensity of the MHD instability is positively correlated with the intensity of the poloidal magnetic field. Furthermore, a preliminary study of the effects of a time-independent pressure profile in the velocity equation has been performed. The presence of the pressure-gradient term may make the plasma instability more complex.

I. INTRODUCTION

Climate change is one of the most challenging threats to human life and some of its effects are already irreversible. The need to find clean alternatives to greenhouse emitting energy production mechanisms is urgent. Nuclear fusion, being sustainable and free from CO_2 emission, is considered as one of the promising future energy resources.

Fusion reactions use deuterium and tritium (isotopes of hydrogen easily found in sea water) to produce nearly four million times [1] more energy than burning coal or gas, and four times as much as nuclear fission without the risk of a nuclear meltdown or dangerous radioactive or polluting waste. These kind of reactions take place in the core of stars, where the gravitational forces keep the hydrogen confined in a restricted and dense space with extreme temperatures. Under these conditions a state of ionized gas is reached, where nuclei and electrons have too much energy to stay bound. This state is called plasma and it is electrically conductive and, thus, sensitive to magnetic fields.

Since the current world's largest fusion reactor, Joint European Torus (JET), achieved the first ever controlled release of fusion power in 1991, there has been hope that a commercial nuclear reactor could be built in the near future. Scientists from countries around the world have joined resources and knowledge in order to better understand the dynamics of fusion reactions and to find a way to achieve a sustained production of electricity. An important landmark was achieved in February 2022 when JET achieved a sustained energy output of 59 megajoules over 5 seconds [2]. This achievement has encouraged the community, as it is a first step towards long lasting energy production.

A. Fusion nuclear reactors

Reproducing a star's core inside a few meters wide reactor is a colossal undertaking. Despite this, fusion reactors achieve confinement using strong external magnetic fields. These fields prevent plasma from directly touching the reactor walls, which would be damaged in the process due to the extremely high temperatures.

There are different designs of fusion reactors. The most relevant ones are the tokamak and the stellarator. The tokamak is the most popular reactor amongst all the options. It consists of a toroidal chamber with surrounding coils which generate toroidal and poloidal magnetic fields. The combination of the two prevents the plasma from touching the vessel's walls, creating a helical magnetic field with a toroidal component and a toroidal flow of the plasma. The stellarator has also a toroidal configuration. Its magnetic field is much more complex because it is generated by coils which are not toroidally symmetric. This complicated configuration is designed to reduce the plasma instabilities present in tokamaks and other machines. The main issue with this design is the difficulty of manufacturing the coils due to its complex shape.

The reactor type considered in this work corresponds to linear machines, which use cylindrical chambers instead of toroidal ones. In this type of chamber, magnetically confined plasma has several MHD scale instabilities such as *Z-pinch* or *θ-pinch*. In the *Z-pinch* instability, the current runs through the plasma parallel to the Z axis of the cylinder, while the magnetic field is azimuthal. In the *θ-pinch* configuration, the electric field is in the azimuthal direction and the magnetic field lines are parallel to the Z axis. The result for both cases is similar: according to the Lorentz force, plasma will be compressed along the axis. The combination of *Z-pinch* and *θ-pinch* yields the so called "screw-pinch" which is the one studied in this work.

II. MAGNETOHYDRODYNAMICS (MHD)

When the plasma dynamics are modelled, two main features must be considered. On the one hand, plasma is an ionized gas, so it is susceptible to magnetic and electric fields. On the other hand, the medium studied is a fluid, therefore it follows classical fluid dynamics. This means

that the dynamical equations for the plasma combine conventional fluid dynamics and Maxwell's electromagnetism laws. This combination yields the visco-resistive MHD equations, which are the Navier-Stokes equation with the Lorentz force (1) and the induction equation (2), which combines Ohm's law, Faraday's equation and Ampère's law. These equations read (using normalized velocity by Alfven's velocity $C_a = \frac{B_0}{\sqrt{\rho\mu_0}}$ and a reference magnetic field B_0.):

$$\frac{\partial \boldsymbol{B}}{\partial t} = (\boldsymbol{B}\cdot\nabla)\boldsymbol{u} - (\boldsymbol{u}\cdot\nabla)\boldsymbol{B} + \lambda\nabla^2\boldsymbol{B} \tag{1}$$

$$\frac{\partial \boldsymbol{u}}{\partial t} = (\boldsymbol{B}\cdot\nabla)\boldsymbol{B} - \frac{1}{2}\nabla\boldsymbol{B}^2 - (\boldsymbol{u}\cdot\nabla)\boldsymbol{u} + \nabla^2(\nu\boldsymbol{u}) - \nabla P \tag{2}$$

Here, $\boldsymbol{B}$ is the magnetic field and $\boldsymbol{u}$ is the velocity field. Also, λ corresponds to the magnetic diffusivity and ν to the kinematic viscosity. These equations are non-linear and have non-analytical solution. In addition, they are tightly coupled by $\boldsymbol{B}$ and $\boldsymbol{u}$, as they appear in both equations and they depend on each other. The non-linear coupling of the magnetic and velocity fields creates a MHD dynamo effect which converts the kinetic energy into magnetic energy. This process includes the self-organization of the plasma [3]. The characteristics of these structures will be discussed in the following sections of this work.

III. OPENFOAM

In order to solve the MHD equations, the OpenFOAM software [4] has been used. OpenFOAM is a free computational fluid dynamics (CFD) software which can solve the dynamical equations for different types of fluids. The source code is written in *C++* and the software is open source, which means that the existing solvers can be modified to fit the needs of any specific case.

OpenFOAM is divided in three main parts:

- The **mesh** is the grid of points that define the spatial domain of the case. At each of these points, the specified vector and scalar fields take a defined value which evolves in each time step.
- The **solver** is the part of the program used to define and run the numerical methods to solve the equations for a given time and time step. The size of the time step is very important in order to find the balance between precision and computational time.
- The **initial conditions** are given in each case and are the input to the solver in order to start the simulation. The initial conditions and boundary conditions are extremely important for the evolution of the simulation.

In order to visualize each saved time slice, *Paraview* [5] has been used, which is a program capable of plotting the resulting fields in the mesh and visualising the case.

IV. THE CASE: PLASMA CONFINED IN A CYLINDER BY A MAGNETIC FIELD

In this project, the simulated case consists of an electrically conducting fluid (plasma) confined inside of a cylinder by a helical magnetic field imposed at boundary. In cylindrical coordinates, its components are:

$$\boldsymbol{B} = (B_r, B_\phi, B_z) = (0, \frac{B_{wall}}{R_i}r, B_{axis}) \tag{3}$$

where R_i is the internal radius of the cylinder and B_{wall} and B_{axis} are the values of the azimuthal magnetic field at the cylinder wall and the constant magnetic field in the axial direction respectively. The MHD equations are dimensionless, therefore, the magnetic field values are given in units of a reference magnetic field. The importance of the relation between the magnitude of these last two values is studied and discussed in the following sections.

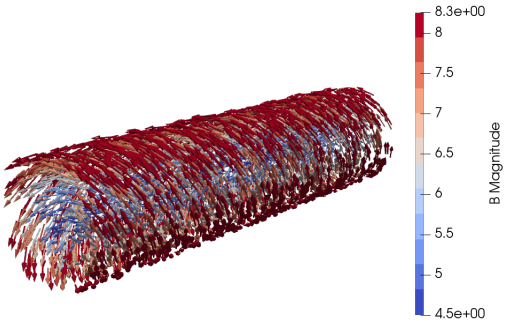

FIG. 1: Field vectors for the initial magnetic field with $B_{wall} = 7.0$ and $B_{axis} = 4.5$.

A. Simulation set-up

At the side wall of the cylinder, no-slip (and non penetration) boundary condition is applied. The cylinder is periodic at both ends (infinite periodic cylinder). For the inital condition, an uncorrelated gaussian solenoidal velocity field is imposed, with kinetic energy of the order 10^{-7}. The kinematic viscosity and magnetic resistivity are set to $\nu = \lambda = 0.02$ for all cases.

The simulation geometry consists of five sub-domains. Each domain has $(30, 30, 150)$ grid points in the (x,y,z) directions respectively. The time step used in the time-integration is 0.001(the dimensions of time are irrelevant, so they will be treated as arbitrary units $(a.u)$).

B. Effect of the toroidal and poloidal magnetic field ratio.

The pressure in this section is set as constant, therefore $\nabla P = 0$ in equation (2). A pressure profile will be introduced later on in order to study its effect on the MHD flow as discussed in the next section.

In this work, the dependence of the magnetic field on the MHD energy has been studied. Among the physics parameters used in this work, it is observed that when $B_{axis} > B_{wall}$ the dominating part of the magnetic field is the axial one. This means that the *Z-pinch* mode is dominant, while in the case where $B_{axis} < B_{wall}$ the *θ-pinch* mode is the strongest. To see the effect of this change in pinch dominance, different cases have been analysed for $B_{wall} < B_{axis}$ and $B_{wall} > B_{axis}$. The simulations have been performed from time $t = 0$ to $t = 10$.

In order to compare the cases, $B_{axis} = 4.5$ is fixed, and B_{wall} is varied from $B_{wall} = 3.0$ to $B_{wall} = 10.0$. The larger values of B_{wall} ($B_{wall} > 10$) crashed the simulation due to mesh quality limitations. Despite this inconvenience, the results obtained give an overall idea of the behaviour of the plasma. The magnetic, total and kinetic energies of the plasma need to be studied in order to see whether there are any instabilities.

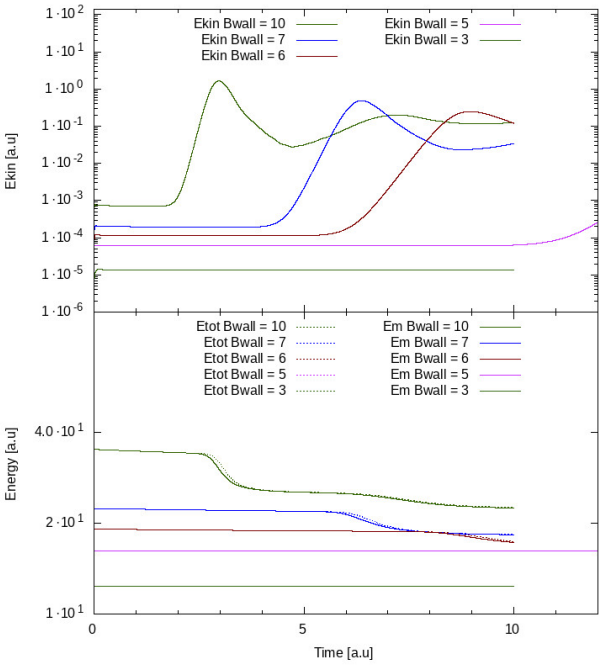

FIG. 2: Top panel: Evolution of kinetic energies with time for $B_{axis} = 4.5$ and $B_{wall} = 3$, 5, 6, 7 and 10. Bottom panel: Evolution of the potential and magnetic energies with time for the above mentioned B_{wall} and B_{axis} values. The vertical axis is logarithmic in both cases.

Figure 2 shows that for $B_{wall} = 3$, no instabilities are observed within the time range considered compared to the other studied values of B_{wall}. Therefore, the kinetic energy is constant during all the simulation resulting in a stable plasma without any abrupt behavior. For the other cases, plasma is stable until an instability develops and the kinetic energy rises abruptly. After reaching a peak, it later relaxes to start rising again at a slower rate. For $B_{wall} = 10$, looking at the bottom part of Figure 2, for example, before around $t = 3$ both the magnetic and total energies are practically identical. This is because the kinetic energy is very low and therefore, its contribution to the total energy, $E_{tot} = E_{kin} + E_{mag}$, is negligible. When the instability triggers, both energies drop and the magnetic and total energies no longer coincide. An exchange between magnetic and kinetic energy has been produced. In addition to this, the total energy is no longer constant and drops. This effect is produced because the dissipative terms of the MHD equations (1 and 2) used in this work are large due to computational limitation. The structure formation of the velocity field is discussed in the next section.

For higher B_{wall} values, these peaks happen earlier in the simulation, meaning that the plasma is stable for less time before it develops the helical flow. As B_{wall} increases, each peak gets higher so the maximum value of the kinetic energy increases. This leads to more intense instabilities as B_{wall} grows.

For the total and magnetic energies, as B_{wall} increases, the total energy loss due to dissipation is also larger. The difference between both energies when instabilities occur also increases with B_{wall} because, as mentioned before, the kinetic energy of the helical streams also grows.

Among the physics parameters used in this work, it is observed that when $B_{wall} > B_{axis}$, a MHD dynamo event is observed. A more detailed analysis is beyond the scope of this work and should be carried out in the future.

C. Implementation of an initial pressure profile

In the previous section, the pressure gradient has been ignored in equation (2). Now, the effect of a pressure profile will be considered. The first approximation is to implement a time independent pressure profile:

$$P(r) = \frac{B_{wall}^2}{a^2}(a^2 - r^2) \tag{4}$$

where a is the internal radious of the cylinder. This is a simple parabolic pressure profile which has been chosen to meet the magnetostatic equilibrium condition, when the Lorentz force and the force due to the pressure gradient are equal and opposite:

$$\nabla P = \boldsymbol{J} \times \boldsymbol{B} \tag{5}$$

where $\boldsymbol{J} = \nabla \times \boldsymbol{B}$ is the current density. The simulation has been performed until $t = 20$ to see the behavior of the plasma in later time steps and to better compare the cases with and without pressure gradient.

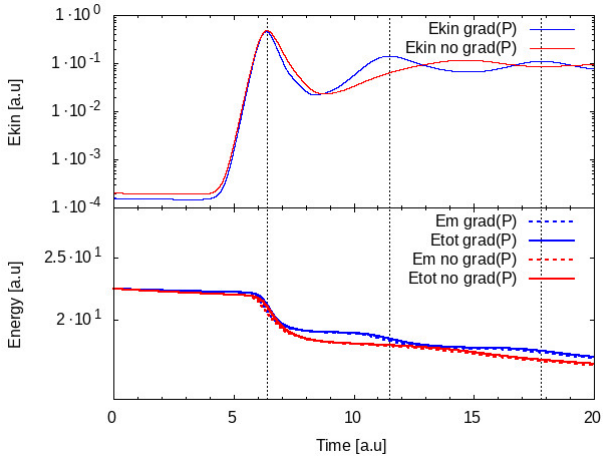

FIG. 3: Top panel: kinetic energy evolution in time for the case with ∇P (blue) and without ∇P (red). Bottom panel: total (filled lines) and magnetic (dotted lines) energy evolution in time for the case with and without pressure gradient. The vertical axis is logarithmic in both cases. Vertical dotted lines correspond to the maximums in the kinetic energy ($t \approx 6.4$, 11.5 and 17.8) for the case with pressure gradient.

In Figure 3, for the kinetic energies (top), it can be seen that the absolute maximum kinetic energy is located at the same time in both cases. After the first peak, an oscillating behaviour is observed for both cases. This is due to the dominance of the non-linear terms of the MHD equations in the simulation. This justification could be verified analysing the energies corresponding to each non-linear term separately (spectrum analysis), however this would lead to an overly advanced analysis of the case, which will be left for future studies. The tendency of the oscillations in both cases is to stabilize on a determined value of the kinetic energy.

The main difference between the two kinetic energy profiles (top) in Figure 3 is the frequency of the oscillations. The case with pressure gradient oscillates with a higher frequency than its counterpart, kick-starting the second instability earlier than the line without ∇P. This last case is much smoother instead and it is more stable, triggering less and more shallow instabilities overall.

Comparing the total and magnetic energies for both cases in Figure 3, each step in the bottom profile corresponds to an instability and a peak in the kinetic energy. For the first helical formation (first kinetic energy peak), the instability without pressure gradient lasts longer than the one with pressure gradient, thus dissipating more energy in the first instability.

Helical structures form along the cylinder. The isosurfaces in Figure 4 reproduce the behavior observed in Roberts' paper [6]. The aim of this part of the work is to see how these structures evolve in time and how the presence of pressure gradient affects their characteristics.

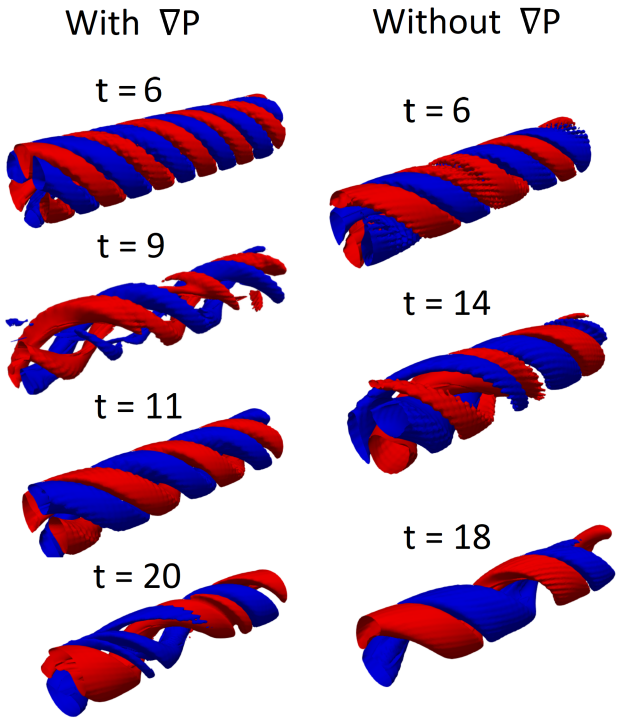

FIG. 4: Isosurfaces for the axial velocity $u_z = \pm 0.2$ where the red and blue colors correspond to the positive and negative directions of u_z respectively. Left: helical structures formed around $t = 6$, $t = 9$, $t = 11$ and $t = 20$ for the case with pressure gradient. Right: helical structures formed around $t = 6$, $t = 14$ and $t = 18$ for the case without pressure gradient.

In Figure 4, the different helical structures observed in the simulations with and without pressure gradient are presented. It can be seen that the number of helices of each structure reduces as plasma relaxes and time evolves. Comparing now the cases with and without pressure gradient, it is observed that the addition of the pressure profile plays a role on the structure of the collective behavior. In the first structure corresponding to the first instability ($t = 6$), despite having nearly the same kinetic energies, the case with pressure gradient presents six helices, while in the setting without ∇P, the structure shows only four helices.

Considering now the structures obtained for different times and comparing them to the kinetic energy profile in Figure 3, the behavior of these oscillating helical modes can be studied. Near the kinetic energy minima, plasma velocity is low, leading to a loss of homogeneity in the shapes of the isosurfaces ($t = 9$). After the kinetic energy minima, the velocity rises and the kinetic energy eventually reaches the next peak, near to which the structures are smoother and better defined ($t = 11$). After reaching the peak, the kinetic energy lowers again to another minimum completing an oscillation. In Figure 4, between

the peaks of $t = 6$ and $t = 11$, a transition in the structure has occurred in $t = 9$, when the number of helices has decreased from six to four. This transition happens near a minimum in the kinetic energy. For the case without ∇P, another transition is observed for $t = 14$ where the number of helices decreases from four to two. As plasma relaxes the helical structures become more stable in time and transitions occur less frequently, presenting more than one oscillation between each transition. Eventually, plasma reaches a steady state.

Comparing again the two setups, the third structure for the case with pressure gradient ($t = 11$) has the same number of helices as the first one of the case without pressure gradient ($t = 6$) despite having very different kinetic energies. Lastly, for $t = 20$ with ∇P, the structure is transitioning to a state with two helices similar to the stable one of $t = 18$ in the case without the pressure gradient.

V. CONCLUSIONS

The MHD dynamics in the magnetically confined plasma in cylindrical geometry has been studied. Analysing the total, magnetic and kinetic energy evolutions, it has been seen that, when the poloidal component of the magnetic field (B_{wall}) is increased, a MHD dynamo action which converts the kinetic energy to magnetic energy is observed. This behavior is caused by the non-linear terms in the MHD equations and the coupling between them through $\boldsymbol{B}$ and $\boldsymbol{u}$. During the MHD dynamo, a helical structure of the velocity field is observed.

In this work, a preliminary approach of a time-independent pressure profile has been implemented to the MHD system used in OpenFOAM. In the non-linear state, the MHD energy shows oscillations in the relaxation process. In the presence of the time-independent pressure profile, the frequency of the oscillations becomes larger than the one in the absence of pressure profile. The analysis of the velocity field helical structures has shown that the number of streamlines tends to decrease in time during the MHD relaxation process.

In the future, the pressure evolution equation needs to be implemented. The plasma pressure plays an important role on the MHD stability, making its physics more complex. Further investigation such as spectrum analysis should be performed to quantify the MHD behavior.

Acknowledgments

I would like to thank my supervisors, Dr. Shimpei Futatani and Dr. Assumpta Parreño, for all the good advice and guidance throughout this project. I would also like to thank my family and friends for their unconditional support.

[1] ITER website, "Advantages of fusion", `https://www.iter.org/sci/Fusion`
[2] World Nuclear News, URL: `https://www.world-nuclear-news.org/Articles/Fusion-energy-record-at-JET-huge-step-forward`
[3] Shimpei Futatani, Jorge A. Morales, and Wouter J. T. Bos , "Dynamic equilibria and magnetohydrodynamic instabilities in toroidal plasmas with non-uniform transport coefficients", Physics of Plasmas 22, 052503 (2015)
[4] OpenFOAM website: `https://openfoam.org/`
[5] Paraview website: `https://www.paraview.org/`
[6] M. Roberts, M. Leroy, J. Morales, W. Bos and K. Schneider, "Self-organization of helically forced MHD flow in confined cylindrical geometries", Fluid Dynamics Research, 46, 061422 (2014) `https://iopscience.iop.org/article/10.1088/0169-5983/46/6/061422/meta`
[7] Jorge A. Morales, "Confined magnetohydrodynamics applied to magnetic fusion plasmas", Doctoral theses, theses director: Wouter J.T. Bos (2013)
[8] Chahine, R., "MHD simulations of the Reversed Field Pinch", Doctoral theses, theses director: Wouter J.T Bos (2017)
[9] McCracken, G., Stott, P., "Fusion, the energy of the universe", (Academic Press, 2012, 2nd. ed.)